Functional Representation for the Born−Oppenheimer Diagonal Correction and Born−Huang Adiabatic Potential Energy Surfaces for Isotopomers of H_3[†]

Steven L. Mielke,*[,‡] David W. Schwenke,[§] George C. Schatz,[‡] Bruce C. Garrett,[∥] and Kirk A. Peterson[⊥]

Department of Chemistry, Northwestern University, Evanston, Illinois 60208-3113, NASA Ames Research Center, MS T27B, Moffett Field, California 94035-1000, Chemical and Materials Sciences Division, Pacific Northwest National Laboratory, Richland, Washington 99352, Department of Chemistry, Washington State University, Pullman, Washington 99164-4630

Received: December 16, 2008; Revised Manuscript Received: February 13, 2009

Multireference configuration interaction (MRCI) calculations of the Born−Oppenheimer diagonal correction (BODC) for H_3 were performed at 1397 symmetry-unique configurations using the Handy−Yamaguchi−Schaefer approach; isotopic substitution leads to 4041 symmetry-unique configurations for the DH_2 mass combination. These results were then fit to a functional form that permits calculation of the BODC for any combination of isotopes. Mean unsigned fitting errors on a test grid of configurations not included in the fitting process were 0.14, 0.12, and 0.65 cm^{-1} for the H_3, DH_2, and MuH_2 isotopomers, respectively. This representation can be combined with any Born−Oppenheimer potential energy surface (PES) to yield Born−Huang (BH) PESs; herein, we choose the CCI potential energy surface, the uncertainties of which (∼0.01 kcal/mol) are much smaller than the magnitude of the BODC. Fortran routines to evaluate these BH surfaces are provided. Variational transition state theory calculations are presented comparing thermal rate constants for reactions on the BO and BH surfaces to provide an initial estimate of the significance of the diagonal correction for the dynamics.

1. Introduction

The H_3 system, together with its various isotopologs, is an important archetype for understanding chemical reactivity, and the experimental and theoretical study of it has both a storied history[1−7] and an ongoing saga. The Born−Oppenheimer[8] (BO) potential energy surface (PES) for this system is the best characterized[9−11] of any chemical reaction, but in important cases, non-Born−Oppenheimer effects must be addressed for theoretical calculations to yield conclusive results; the calculation of low-temperature thermal rate constants[12] is one example of where the need to address non-BO effects has already been demonstrated.

At energies well below those of the first excited electronic state, adiabatic corrections can account for the dominant errors resulting from the BO approximation. The most common adiabatic correction consists of adding a Born−Oppenheimer diagonal correction (BODC) to the BO PES to yield what is referred to[13] as the Born−Huang[14] (BH) energy. The BODC, which is sometimes referred to as a nuclear-motion correction, is the first-order perturbation correction to the electronic energy due to the finite mass of the nuclei. In our calculations, it is calculated as $\langle\Psi_i|\mathbf{T}_N|\Psi_i\rangle$, where $\mathbf{T}_N$ is the nuclear kinetic energy operator in space-fixed Cartesian coordinates and $|\Psi_i\rangle$ denotes a BO electronic state. In contrast to the BO surface, the BH surfaces are mass-dependent; the functional representation we present below yields diagonal corrections for any possible mass combination.

The BO and BH energies of the ground state are lower and upper bounds, respectively, on the exact ground-state energy (as well as any other adiabatic approximation). Other,[15−17] and arguably better, adiabatic approximations exist, with the minimal adiabatic approximation[16] (MAA) of Golden being especially noteworthy from a formal perspective (MAA surfaces do not exhibit conical intersections or geometric phase effects), but these approximations are significantly harder to calculate and have not yet been implemented in electronic structure packages. At configurations with energies well below those of the excited states, the BH approximation should be significantly more accurate than the BO approximation, but this is not true everywhere; for instance, the BH energy is singular at points of conical intersection and too large near intersection seams. Another example is in the asymptotic H + H + H region, where the lowest two electronic states become nearly degenerate. This near degeneracy leads to an extremely slow approach, with increasing separation, of the BODC to the asymptotic limit of three times the H-atom value. Before this limit can be reached in practice, numerical issues make the computations difficult because the interactions of the H atoms become so small that the configuration mixing coefficients are not well determined. The presence of these features presents a significant challenge for fitting the BODC to a global functional form. The goal of the present study is to provide a functional representation that will yield accurate adiabatic corrections for all regions of the PES that are accessible in calculations for which dynamical treatments involving only a single electronic state are appropriate. Thus, we do not attempt a globally accurate representation, which would include regions near the conical intersection seams, because nonadiabatic effects would then also need to be addressed, which is a substantially more demanding task.

[†] Part of the "George C. Schatz Festschrift".

* Corresponding author. E-mail: slmielke@gmail.com.
[‡] Northwestern University.
[§] NASA Ames Research Center.
[∥] Pacific Northwest National Laboratory.
[⊥] Washington State University.

10.1021/jp8110887 CCC: $40.75
Published on Web 03/16/2009

We begin by reviewing relevant details of the BO PES and the diagonal correction in Section 2. In Section 3, we describe the ab initio calculations and the functional representation of the diagonal correction. In Section 4, we analyze the fitted surfaces as well as the BH surface that results when the correction surface is added to the BO surface, and in Section 5, we provide some concluding remarks.

2. Background

2.1. BO Surfaces. Several noteworthy analytical PESs[10,18−21] have been presented for the H_3 system; the most accurate of these is the CCI PES,[10] which was fitted to energies of 4066 configurations that were obtained via a highly accurate many-body basis set extrapolation[9] employing essentially full configuration interaction (FCI) quality (accurate to within $\sim 1\ \mu E_h$) multireference configuration interaction (MRCI) calculations primarily with data obtained using the aug-cc-pVTZ and aug-cc-pVQZ basis sets.[22,23] The CCI surface is estimated to be globally accurate to within ~0.01 kcal/mol, with most of the remaining uncertainty due to residual errors in the basis set extrapolation. This PES has a collinear reaction path with a barrier at $R_1 = R_2 = 1.7572$ a_0 of 9.602 kcal/mol. The most accurate estimate of the barrier height,[10,11] which was obtained via basis set extrapolations employing basis sets as large as octuple zeta, is 9.608 kcal/mol (with an absolute energy of $-1.659\ 165\ E_h$); the most recent[24] quantum Monte Carlo barrier energy estimate of $-1.659\ 165\ E_h \pm 1.5\ \mu E_h$ agrees perfectly with this estimate. Relativistic corrections to the H_3 barrier height have been estimated[10] to be only $\sim 0.05\ cm^{-1}$.

At D_{3h} (equilateral triangle) configurations with $R_1 = R_2 = R_3 = 0.94$ a_0, the ground and first excited states exhibit a conical intersection.[10] At $R_1 = R_2 = R_3 = 0.94$ a_0, the first three electronic states are degenerate, and at more compact configurations, the D_{3h} conical intersection seam continues between the first two excited states. The lowest energy D_{3h} conical intersection is at $R_1 = R_2 = R_3 = 1.97$ a_0 and lies 2.696 eV above the $H + H_2$ (R_{eq}) zero of energy. The system also exhibits a C_{2v} conical intersection seam, a portion of which involves the ground and first excited states and a portion of which involves the first two excited states,[10] but the lowest-energy configuration on this seam lies more than 10 eV above the $H + H_2$ (R_{eq}) zero of energy, so this seam can be neglected for the present purposes.

2.2. BO Diagonal Correction. The Born−Oppenheimer approximation begins by writing the Hamiltonian, **H**, of the system as

$$\mathbf{H} = \mathbf{T}_N + \mathbf{H}^{BO} \tag{1}$$

where $\mathbf{T}_N$ is the nuclear kinetic energy operator given by

$$\mathbf{T}_N = -\sum_\alpha \frac{\hbar^2}{2m_\alpha}\nabla_\alpha^2 \tag{2}$$

where m_α is a nuclear mass. One then solves

$$\mathbf{H}^{BO}|\Psi_i\rangle = V_i^{BO}|\Psi_i\rangle \qquad i = 1, 2, 3... \tag{3}$$

where V_i^{BO} is the Born−Oppenheimer PES for state i that depends only on the nuclear coordinates. The nuclear kinetic energy operator couples the BO eigenstates so the exact system cannot be represented by PESs. However, diagonal terms given by

$$G_{ii} = \langle\Psi_i|\mathbf{T}_N|\Psi_i\rangle \tag{4}$$

introduce no nonadiabatic coupling and can be added to the BO PESs, leading to what are usually referred to[13] as Born−Huang[14] surfaces, V_i^{BH}, where

$$V_i^{BH} = V_i^{BO} + V_i^{BODC} = V_i^{BO} + G_{ii} \tag{5}$$

Because the BODC is mass-dependent, it will be convenient to represent the BH surface as a sum of two separately fitted surfaces; in the following, we will choose the CCI PES for the BO term.

The BODC is a positive definite quantity, and isolated atoms have significant values (59.7648 cm^{-1} for a H atom). Thus, the geometry dependence of the BODC can be much smaller than its magnitude; for example, at an internuclear separation of $R = 1.40$ a_0, the BODC of H_2 is 114.59 cm^{-1}, which is only 4.94 cm^{-1} less than the sum of the values for two isolated H atoms. As the spacing between electronic states decreases, the derivative couplings and, thus, the BODC tend to increase. Because transition states tend to occur in the neighborhood of widely avoided intersections of two quasidiabatic surfaces, one with reactant bonding character and one with product bonding character, the BODC tends to be systematically larger at transition states than at reactants or products. Therefore, there is a strong tendency for reaction rates to be lower when calculated on a BH surface than on the associated BO surface. For $H + H_2$, the barrier-height correction resulting from the BODC is 0.153 kcal/mol; this is an order of magnitude larger than the remaining uncertainties of the CCI PES and is sufficiently large that it must be accounted for in predicting low-temperature reaction rates.[12]

3. BODC Analytical Potential

3.1. Ab Initio Benchmarks. Most ab initio calculations of the BODC for systems larger than two-electron problems have been limited to implementations at the Hartree−Fock self-consistent field (SCF) level using either spin-restricted[25,26] or unrestricted[27,28] wave functions. Recently, however, numerical implementations allowing BODC calculations have been presented that employed multiconfiguration SCF,[29] single-reference configuration interaction (CI),[30,31] multireference CI (MRCI),[32−35] coupled cluster,[31] and first-order (MP1) [note that although the MP1 correction is zero for the BO energy, it provides a good estimate of the BODC] and second-order (MP2) Møller−Plesset perturbation theory methods.[28,36]

An extensive set of benchmark calculations has already been presented elsewhere for the BODC at the H_3 saddle point[11] and for H_2 and H_3^+ for a wide range of configurations.[11,37−39] Here, we will concentrate on the level of treatment needed to provide accurate data across the entire targeted region of the H_3 PES. As discussed previously,[11] the BODC is best calculated with basis sets that include diffuse functions but otherwise, the level of correlation treatment and basis set sizes needed for accurate evaluation are significantly less stringent than those required for the BO energies. The basis set convergence of the BODC obeys the same $1/l_{max}^3$ dependence,[40−43] (where l_{max} is the largest angular momentum used in the basis) as the BO energies do, but the convergence with respect to the degree of radial completeness is significantly more favorable than that for the

BO energies. The aug-cc-pVTZ basis set[22,23] was sufficient to converge the BODC at the H_3 saddle point to within 0.2 cm^{-1} of the complete basis set limit. The treatment of electron correlation is also less demanding than for the BO energies, and MRCI calculations with only a valence reference space were observed to lie within less than 0.1 cm^{-1} of the FCI limit at the H_3 saddle point, which is more than 2 orders of magnitude greater accuracy than such calculations achieve for the BO correlation energy.

For the calculations presented herein, the BODC will be calculated via the method of Handy et al.[26] using a modification[29,35] of the internally contracted[44,45] MRCI (icMRCI) code of the MOLPRO suite[46] of electronic structure programs. For all the calculations considered here, the internal contraction scheme does not lead to any reduction in the number of configurations; therefore, the results are identical to those of standard MRCI calculations, and we will drop the "ic" prefix henceforth. We consider MRCI calculations employing either a valence (3 orbital) reference space, denoted MRCI(3), or an extended (11 orbital) reference space, denoted MRCI(11), where the orbitals were obtained from complete active space self-consistent field (CASSCF) calculations with active spaces of 3 and 11 orbitals, respectively. Prior MRCI(11) calculations[11] of the BODC at the H_3 saddle point agreed with FCI calculations to within better than 0.01 cm^{-1}. The MRCI(11) calculations are similar to those employed in the calculation of the CCI PES, which were demonstrated[10] to yield results that agreed with FCI calculations of the BO energy to within better than 1 μE_h for a wide range of configurations, except that those calculations used CI natural orbitals rather than the CASSCF orbitals employed here. We use augmented[23] correlation consistent[22] basis sets of either triple-ζ (aug-cc-pVTZ) or quadruple-ζ (aug-cc-pVQZ) quality for all the calculations presented here.

In Table 1, we present BODC calculations at a selection of representative configurations calculated with four levels of treatment: MRCI(3)/aug-cc-pVTZ, MRCI(11)/aug-cc-pVTZ, MRCI(3)/aug-cc-pVQZ, and MRCI(11)/ aug-cc-pVQZ (the cost ratios of these treatments are approximately 1:10:17:70, respectively). These results are sorted in increasing order on the basis of the magnitude of the BO energy, as estimated from the CCI PES, which is also tabulated. The data calculated with the aug-cc-pVTZ basis set agree with those calculated with the aug-cc-pVQZ basis set to within less than 0.8 cm^{-1}, and the agreement is best for the low-energy configurations. Additionally, FCI/aug-cc-pVTZ calculations of the H_2 BODC agree with the accurate results of Wolniewicz[37] to within 0.23 cm^{-1} for $R = 1.2$ a_0, but the level of agreement worsens to 0.43, 0.68, and 1.37 cm^{-1} at 1.1, 1.0, and 0.8 a_0, respectively. Prior benchmark calculations[11] suggest that the basis-set-incompleteness error at the aug-cc-pVQZ basis is quite small (<0.1 cm^{-1} at the H_3 saddle point); thus, the aug-cc-pVTZ H_3 BODC calculations for configurations where all H−H distances exceed 1.2 a_0 seem to typically be within ~0.3 cm^{-1} of the complete basis set limit. For configurations where the BO energy is below 2 eV (with the zero of energy taken as one H infinitely separated from H_2 at its equilibrium separation), the MRCI(3) BODC calculations agree with the MRCI(11) calculations (which are expected to be tantamount to FCI for the BODC) to within 0.3 cm^{-1}; however, for high-energy configurations, especially those near the conical intersection seams, the CI error of the MRCI(3) calculations can be several cm^{-1}. The benchmark calculations suggest, however, that even the MRCI(3)/aug-cc-pVTZ treatment is sufficiently accurate for our needs, especially in the lower-energy regions of the PES that we are primarily targeting, and we adopt it for the calculation of the data used to fit the BODC surface.

Nuclear masses are used in the calculations and are obtained by subtracting 1 m_e from the atomic masses (in a.u.) of 1837.153, 3671.483, 5497.921, and 207.768, for H, D, T, and Mu (i.e., muonium), respectively. We note that some authors[47] have advocated using atomic masses in place of the nuclear ones in an attempt to obtain heuristic improvements beyond those of the BH approximation, so care must be taken when comparing results from different groups. Several units of energy are used in this article, and interconversion is achieved using 1 E_h = 27.211 396 1 eV = 627.5096 kcal/mol = 219 474.7 cm^{-1}; for convenience we note here that 1 cm^{-1} ~ 0.0029 kcal/mol ~4.6 μE_h.

3.2. Functional form. The BODC for any isotopomer of H_3 can be simply expressed via

$$V^{m_1m_2m_3}(R_1,R_2,R_3) = \sum_{i=1}^{3} \frac{A_i(R_1,R_2,R_3)}{m_i} \tag{6}$$

where R_1 is the distance between masses m_1 and m_2, R_2 is the distance between masses m_2 and m_3, and R_3 is the distance between masses m_1 and m_3. Rather than fitting the A_i directly, we instead choose to fit a BODC potential for the DHH mass combination and obtain the A_i values from this potential by solving

$$\begin{pmatrix} 1/m_D & 1/m_H & 1/m_H \\ 1/m_H & 1/m_D & 1/m_H \\ 1/m_H & 1/m_H & 1/m_D \end{pmatrix} \begin{pmatrix} A_1(R_1,R_2,R_3) \\ A_2(R_1,R_2,R_3) \\ A_3(R_1,R_2,R_3) \end{pmatrix} = \begin{pmatrix} V^{DHH}(R_1,R_2,R_3) \\ V^{HDH}(R_1,R_2,R_3) \\ V^{HHD}(R_1,R_2,R_3) \end{pmatrix} \tag{7}$$

By symmetry, we have

$$V^{DHH}(R_1,R_2,R_3) = V^{DHH}(R_3,R_2,R_1) = V^{HDH}(R_1,R_3,R_2) = V^{HDH}(R_2,R_3,R_1) = V^{HHD}(R_2,R_1,R_3) = V^{HHD}(R_3,R_1,R_2) \tag{8}$$

thus, the BODC for any other mass combination can be calculated from three evaluations of our fit for the special case of DHH by using eqs 6−8.

For convenience, we choose to fit the DHH BODC potential using a many body expansion

$$V^{DHH}(R_1,R_2,R_3) = V_0 + V^{DH}(R_1) + V^{HH}(R_2) + V^{DH}(R_3) + V_{3C}(R_1,R_2,R_3) \tag{9}$$

The one-body term, V_0, is equal to the sum of the BODC for the three isolated atoms. The H-atom BODC obtained with the aug-cc-pVTZ basis set is 59.6818 cm^{-1}, which can be compared to the exact value of $(\hbar^2/2m_H) = 59.7648$ cm^{-1}. The HH two-body potential was fit to an extended Rydberg potential,[48]

$$V^{HH}(R) = \exp(-\alpha R)\sum_{j=1}^{14} c_j R^{j-1} \tag{10}$$

and two-body interactions for other mass combinations can be obtained via

TABLE 1: Benchmark BODC Calculations (in cm^{-1}) at Selected Levels of Theory

R_1 (a_0)	R_2 (a_0)	θ	BO energy (eV)[a]	MRCI(3)/ aug-cc-pVTZ	MRCI(11)/ aug-cc-pVTZ	MRCI(3)/ aug-cc-pVQZ	MRCI(11)/ aug-cc-pVQZ
1.4	4.0	180	0.0228	174.73	174.75	174.87	174.89
1.2	5.0	120	0.2633	181.20	181.20	181.58	181.58
1.757	1.757	180	0.4164	227.82	227.78	227.88	227.83
1.6	2.4	120	0.5048	194.06	194.15	194.09	194.17
1.8	2.4	90	1.0762	203.31	203.37	203.33	203.37
1.4	1.4	120	1.6407	252.97	252.73	253.14	252.89
1.0	2.8	80	1.9217	197.59	197.68	198.35	198.45
1.4	1.4	90	2.4004	342.81	341.39	343.04	341.55
2.8	2.8	90	2.6206	253.71	253.52	253.57	253.36
1.2	1.2	180	2.9153	257.43	257.06	258.11	257.72
1.2	1.4	90	3.2004	346.72	345.41	347.19	345.78
1.2	1.2	120	3.3863	285.64	284.59	286.36	285.28
1.2	1.2	100	3.8585	346.40	343.06	347.19	343.80

[a] Calculated with the CCI PES and relative to a zero of energy of $H + H_2$ (R_{eq}).

$$V^{m_1m_2}(R) = \frac{m_H}{2}\left(\frac{1}{m_1} + \frac{1}{m_2}\right)V^{HH}(R) \tag{11}$$

The three-body potential was represented as

$$V_{3C}(R_1, R_2, R_3) = \chi\left[S^{[1]} + CS^{[2]} + G_{11}^{DIM}S^{[3]}\right] \tag{12}$$

The $S^{[\alpha]}$ terms[49] are given by

$$S^{[\alpha]}(R_1, R_2, R_3) = \sum_{\substack{i,j,k=0 \\ i+j+k\neq\max(i,j,k)}}^{i+j+k=11} c_{ijk}^{[\alpha]}\xi_1^i(R_1)\,\xi_2^j(R_2)\,\xi_3^k(R_3) \tag{13}$$

where

$$\zeta_i(R_i) = R_i \exp(-\beta R_i) \tag{14}$$

and symmetry requires that the linear parameters obey

$$c_{ijk}^{[\alpha]} = c_{kji}^{[\alpha]} \tag{15}$$

In principle, we could have chosen to have different nonlinear parameters, β, for the R_{DH} and R_{HH} coordinates, but for the BODC, this would not have led to an appreciable improvement in the quality of the fit.

In eq 12, G_{11}^{DIM} denotes a two-state diatomics in molecules (DIM) solution[50] for the BODC that will be discussed in detail in the following section, C is a cusp emulating term having the form

$$C(R_1, R_2, R_3) = \sqrt{\varepsilon^2 + (R_1 - R_2)^2 + (R_1 - R_3)^2 + (R_2 - R_3)^2} \tag{16}$$

and $\chi(R_1, R_2, R_3)$ is an analytic cutoff function designed to smoothly zero out the three-body potential in regions that are outside the domain of validity of the fit. This cutoff function is given by

$$\chi(R_1, R_2, R_3) = \begin{cases} 0 & s \le \delta_s \text{ or } R_{sum} \le \delta_{R_{sum}} \text{ or } R_i \le \delta_R \text{ for any } i \\ \exp\left(\dfrac{\rho_R}{\delta_{R_{sum}} - R_{sum}} + \dfrac{\rho_R}{\delta_R - R_1} + \dfrac{\rho_R}{\delta_R - R_2} + \dfrac{\rho_R}{\delta_R - R_3} + \dfrac{\rho_R}{\delta_s - s}\right); & \text{otherwise} \end{cases} \tag{17}$$

where

$$R_{sum} = R_1 + R_2 + R_3 \tag{18}$$

and

$$s = \frac{\sqrt{(2R_1^2 - R_2^2 - R_3^2)^2 + 3(R_2^2 - R_3^2)^2}}{(R_1^2 + R_2^2 + R_3^2)} \tag{19}$$

The s variable is a symmetry variable discussed elsewhere;[19,51] the BODC has a pole of order 4 in s at D_{3h} conical intersections, and using this variable in eq 17 is a convenient way to damp out the three-body potential near this intersection seam. The cutoff parameter values were chosen to be $\delta_{Rsum} = 3.3\ a_0$, $\delta_R = 0.72\ a_0$, $\delta_s = 0.25\ a_0$, $\rho_R = 0.02\ a_0$, and $\rho_s = 0.01\ a_0$.

3.3. DIM Solution. In 1985, Garrett and Truhlar presented[50] a two-state DIM approximation for the BODC of a triatomic system. This approximation goes to a constant in each of the atom plus diatom limits (in the case of isotopomers of H_3, it goes to 0 in each arrangement), so it is not appropriate for a globally accurate representation of the BODC. Nevertheless, it has some qualitatively correct features in the strong interaction regime (it also permitted semiquantitative predictions of barrier height corrections resulting from the diagonal correction); thus, it is a convenient shape function to use as part of the functional form for the three-body component of our fitted BODC PES. In the original presentation, the DIM approximation was evaluated numerically via finite differences, but in the present work, we adopt an analytical evaluation.

The DIM Hamiltonian can be written[50]

$$\mathbf{H}^{DIM} = \begin{bmatrix} H_{11} & H_{12} \\ H_{21} & H_{22} \end{bmatrix} \tag{20}$$

with

$$H_{11} = D^{YZ} + V_S^{YZ} + (V_S^{XY} + V_S^{XZ})/4 + 3(V_T^{XY} + V_T^{XZ})/4 \quad (21)$$

$$H_{22} = D^{YZ} + 3(V_S^{XY} + V_S^{XZ})/4 + V_T^{YZ} + (V_T^{XY} + V_T^{XZ})/4 \quad (22)$$

and

$$H_{12} = H_{21} = \sqrt{3}(V_S^{XY} - V_S^{XZ} + V_T^{XZ} - V_T^{XY})/4 \quad (23)$$

where V_S^{XY} and V_T^{XY} are, respectively, the singlet and triplet potentials of diatom XY, and D^{YZ} is the equilibrium dissociation energy of diatom XY. The eigenvalues of $\mathbf{H}^{DIM}$ are

$$V_1^{DIM} = \frac{1}{2}(H_{11} + H_{22}) - \sqrt{\left(\frac{H_{11} - H_{22}}{2}\right)^2 + {H_{12}}^2} \quad (24)$$

and

$$V_2^{DIM} = \frac{1}{2}(H_{11} + H_{22}) + \sqrt{\left(\frac{H_{11} - H_{22}}{2}\right)^2 + {H_{12}}^2} \quad (25)$$

and the eigenvectors are

$$|\Psi_1\rangle = \begin{pmatrix} \sqrt{\frac{1}{2} + \frac{(H_{22} - H_{11})}{4\sqrt{\left(\frac{H_{22} - H_{11}}{2}\right)^2 + {H_{12}}^2}}} \\ \sqrt{\frac{1}{2} - \frac{(H_{22} - H_{11})}{4\sqrt{\left(\frac{H_{22} - H_{11}}{2}\right)^2 + {H_{12}}^2}}} \end{pmatrix} \quad (26)$$

and

$$|\Psi_2\rangle = \begin{pmatrix} -\sqrt{\frac{1}{2} - \frac{(H_{22} - H_{11})}{4\sqrt{\left(\frac{H_{22} - H_{11}}{2}\right)^2 + {H_{12}}^2}}} \\ \sqrt{\frac{1}{2} + \frac{(H_{22} - H_{11})}{4\sqrt{\left(\frac{H_{22} - H_{11}}{2}\right)^2 + {H_{12}}^2}}} \end{pmatrix} \quad (27)$$

The two-state DIM BODC is given by

$$G_{11}^{DIM} = \sum_{i=A,B,C} \frac{-\hbar^2}{2m_i}\langle\Psi_1|\nabla_i^2|\Psi_1\rangle = \sum_i G_{11}^{DIM,m_i} \quad (28)$$

and can be rewritten as a function of the derivative couplings via

$$G_{11}^{DIM,m_i} = \frac{-\hbar^2}{2m_i}\sum_{j=1}^{3}\langle\Psi_1|\frac{\partial}{\partial x_{ij}}|\Psi_2\rangle\langle\Psi_2|\frac{\partial}{\partial x_{ij}}|\Psi_1\rangle = \frac{-\hbar^2}{2m_i}\sum_{j=1}^{3}[f_{12}^{(ij)}]^2 \quad (29)$$

where x_{ij} is the jth Cartesian coordinate of atom i. These expressions can then be transformed into more-convenient expressions given in internal coordinates

$$G_{11}^{DIM,m_A} = \frac{\hbar^2}{2m_A}(\tilde{f}_{12}^{(1)}\tilde{f}_{12}^{(1)} + 2\cos(\theta_{13})\tilde{f}_{12}^{(1)}\tilde{f}_{12}^{(3)} + \tilde{f}_{12}^{(3)}\tilde{f}_{12}^{(3)}) \quad (30)$$

$$G_{11}^{DIM,m_B} = \frac{\hbar^2}{2m_B}(\tilde{f}_{12}^{(1)}\tilde{f}_{12}^{(1)} + 2\cos(\theta_{12})\tilde{f}_{12}^{(1)}\tilde{f}_{12}^{(2)} + \tilde{f}_{12}^{(2)}\tilde{f}_{12}^{(2)}) \quad (31)$$

$$G_{11}^{DIM,m_C} = \frac{\hbar^2}{2m_C}(\tilde{f}_{12}^{(2)}\tilde{f}_{12}^{(2)} + 2\cos(\theta_{23})\tilde{f}_{12}^{(2)}\tilde{f}_{12}^{(3)} + \tilde{f}_{12}^{(3)}\tilde{f}_{12}^{(3)}) \quad (32)$$

where θ_{ij} is the included angle associated with R_i and R_j, and

$$\tilde{f}_{12}^{(i)} = \langle\Psi_1|\frac{\partial}{\partial R_i}|\Psi_2\rangle = \frac{\mathrm{sign}(H_{12})}{(H_{22} - H_{11})^2 + 4{H_{12}}^2} \times \left(H_{12}\frac{\partial(H_{22} - H_{11})}{\partial R_i} - (H_{22} - H_{11})\frac{\partial H_{12}}{\partial R_i}\right) \quad (33)$$

Herein, we adopt the DIM parametrization used previously;[50,52] in particular, the singlet potential is represented as a Morse function,

$$V_S^{ij} = D^{ij}(y^2 - 2y) \quad (34)$$

where

$$y = \exp[-\kappa_{ij}(R_{ij} - R_{ij}^e)] \quad (35)$$

and the triplet is represented by

$$V_T^{ij} = \frac{(1 - \Delta_{ij})}{(1 + \Delta_{ij})}D^{ij}(y^2 + 2y)/2 \quad (36)$$

where the Δ_{ij} are Sato parameters chosen as 0.132, R^e is the equilibrium distance (0.741 287 1 a_0), and the D^{ij} are 109.4583 kcal/mol. A plot of the DIM BODC for collinear H + H_2 is given in Figure 1.

3.4. Data and Fitting. The electronic structure calculations directly yield the A_i values of eq 6, so in selecting configurations at which to evaluate data, we can use permutational symmetry to limit consideration to $R_1 \le R_2 \le R_3$. The primary set of data points was selected by choosing R_1 and R_2 from among {0.8, 1.0, 1.2, 1.4, 1.6, 1.8, 2.0, 2.4, 2.8, 3.4, 4.0, 4.6, 5.0, and 5.5 a_0} and θ from among {180, 170, 160, 150, 140, 130, 120, 110, 100, 90, and 80°}; only points with $R_1 \le R_2 \le R_3$, $R_1 + R_2 +$

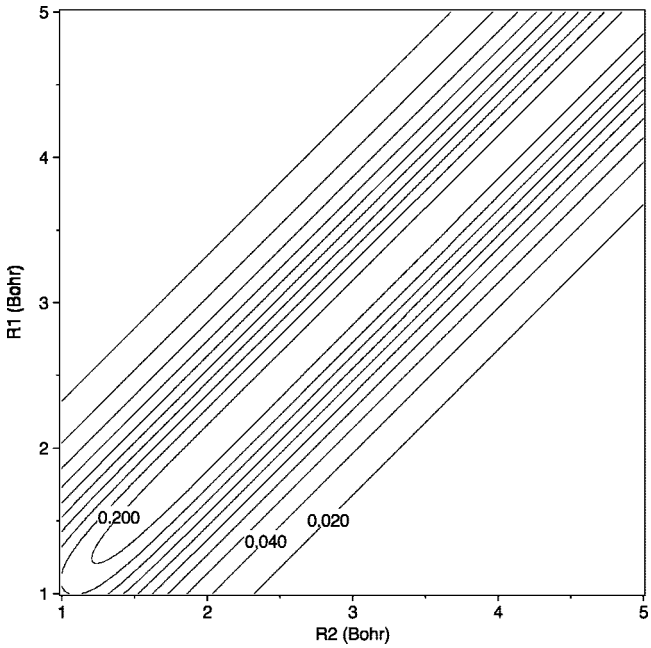

Figure 1. A contour plot of the DIM BODC for the collinear H + H_2 reaction. The contours start at 0.02 kcal/mol and have increments of 0.02 kcal/mol.

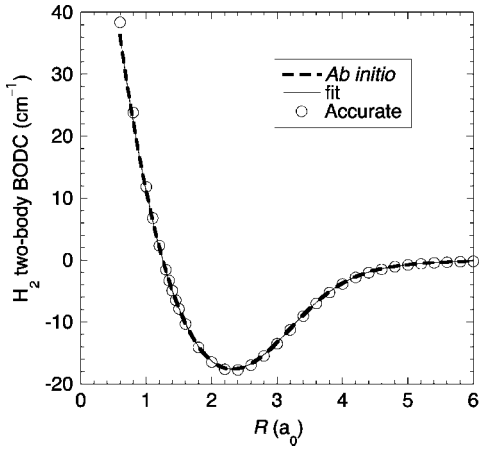

Figure 2. A comparison of the FCI/aug-cc-pVTZ BODC calculations for H_2, the two-body fit of eq 10, and the accurate values of Wolniewicz. All data are tabulated relative to the results for two isolated H atoms.

$R_3 \leq 3.6$ a_0, and $R_1 \leq 2.8$ a_0 were retained. More points were added in the "compact" region with R_1 chosen from {1.1, 1.3, 1.5, 1.7, 1.9 a_0}, R_2 chosen from {1, 1.1, 1.2, 1.3, 1.4, 1.5, 1.6, 1.7, 1.8, 1.9, 2.0 a_0}, and with θ choices and constraints as above. An additional 120 points were chosen along the collinear minimum energy path of the CCI PES with R_1 ranging from 0.76 to 2.95 a_0 in increments of 0.01 a_0, and finally, 10 symmetric collinear points near the saddle point were chosen with R_1 ranging from 1.70 to 1.79 a_0 in increments of 0.01 a_0. This resulted in a set of 1397 configurations at which electronic structure calculations were performed.

The use of permutational symmetry with the calculated ab initio data leads to 4041 symmetry-unique BODC values for the DHH mass combination. The lowest DHH BODC value within this set was 131.66 cm^{-1}; 3315 points had values below 200 cm^{-1}, 656 fell within 200−300 cm^{-1}, 52 fell within 300−400 cm^{-1}, 11 fell within 400−500 cm^{-1}, and 7 points had values exceeding 500 cm^{-1}. These last 7 points were excluded from the fitting process.

TABLE 2: Mean Unsigned Deviations (MUD), Root Mean Square Deviations (RMSD), and Worst Deviations Observed for the BODC of Various Isotopomers on the Set of Configurations Used in the Fitting Process[a]

system	subset	no. points	MUD	RMSD	worst deviation
DH_2	all	4034	0.069	0.114	1.50
DH_2	$E^{BO} < 2$ eV	2900	0.052	0.074	0.47
H_3	all	1394	0.083	0.141	1.56
H_3	$E^{BO} < 2$ eV	999	0.063	0.089	0.51
MuH_2	all	4034	0.409	0.720	13.06
MuH_2	$E^{BO} < 2$ eV	2900	0.299	0.436	3.06

[a] Data are tabulated for the full set as well as for the subset of configurations where the BO energy (calculated with the CCI PES) is less than 2 eV above the H + H_2 (R_{eq}) zero of energy. All values are in cm^{-1}.

TABLE 3: Mean Unsigned Deviations (MUD), Root Mean Square Deviations (RMSD), and Worst Deviations Observed for the BODC of Various Isotopomers on a Test Set of Configurations *Not* Used in the Fitting Process[a]

system	subset	no. points	MUD	RMSD	worst deviation
DH_2	all	805	0.120	0.230	1.70
DH_2	$E^{BO} < 2$ eV	700	0.098	0.155	0.69
H_3	all	280	0.144	0.275	1.94
H_3	$E^{BO} < 2$ eV	242	0.118	0.189	0.78
MuH_2	all	805	0.645	1.138	8.72
MuH_2	$E^{BO} < 2$ eV	700	0.539	0.823	4.34

[a] Data is tabulated for the full set as well as for the subset of configurations where the BO energy is less than 2 eV (calculated with the CCI PES) above the H + H_2(R_{eq}) zero of energy. All values are in cm^{-1}.

BODC calculations were also performed on a supplementary set of configurations that were not used in the fitting process so that the quality of the fitted surface could be rigorously assessed. Configurations were selected with R_1 and R_2 chosen from {1.15, 1.35, 1.55, 1.75, 1.95, 2.2, 2.6, 3.1, 3.7, 4.3, 4.8 a_0}, θ chosen from {175, 155, 135, 115, 95°}, and subject to the constraints of $R_1 \leq 2.8$ a_0 and $R_1 \leq R_2 \leq R_3$. This results in a set of 280 symmetry-unique configurations for H_3 and 805 configurations for DHH.

For the HH potential, a total of 200 FCI/aug-cc-pVTZ calculations of the BODC were used in the fitting, and the resulting mean unsigned and worst errors were 0.0017 and 0.0036 cm^{-1}, respectively. A comparison of the ab initio data, the fitted curve, and accurate results[37] is shown in Figure 2. The agreement between the aug-cc-pVTZ values and the accurate results is excellent except at very small internuclear separations, with the error at 0.6 a_0 being about 2 cm^{-1}.

The least-squares fit of the DHH three-body potential involved 540 linear parameters and 1 nonlinear parameter (the various parameters of the damping function were not simultaneously optimized). As the single nonlinear parameter was varied, the linear parameters were optimized by a call to a linear least-squares routine (which has a deterministic solution); this greatly simplifies the fitting process compared to doing a full nonlinear optimization, and guarantees an optimal result. The observed mean unsigned deviations (MUD), root-mean-square deviations (RMSD), and worst deviations evaluated on the set of configurations used in the fitting process are given in Table 2 for diagonal corrections of various isotopomers. The observed uncertainties are all quite low, although the values are larger for the MuH_2 isotopomer than for the other cases.

Measures of quality based only on the configurations used in the fitting process are notorious for underestimating the true

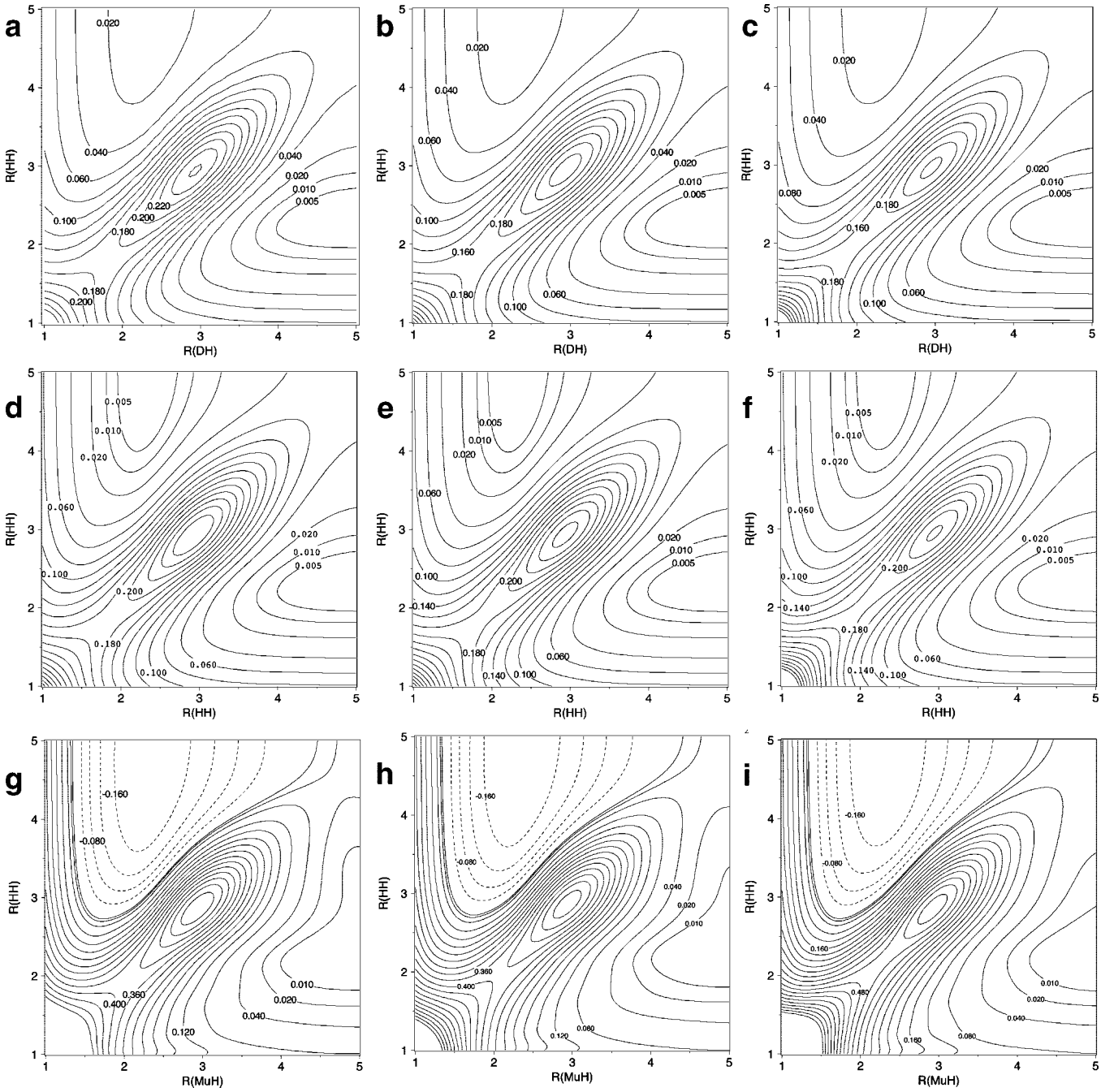

Figure 3. Contour plots of the BODC relative to the minimum diagonal correction at the X + H_2 asymptote for DHH, HHH, and MuHH. Distances are in Bohr and contours are in kcal/mol. For H_3 and DH_2, the contour lines are multiples of 0.02 kcal/mol, except for 0.005 and 0.01; for MuH_2, the contour lines are multiples of 0.04 kcal/mol, except for 0.01 and 0.02. (a) DHH at $\theta = 180°$, (b) DHH at $\theta = 150°$, (c) DHH at $\theta = 120°$, (d) H_3 at $\theta = 180°$, (e) H_3 at $\theta = 150°$, (f) H_3 at $\theta = 120°$, (g) MuHH at $\theta = 180°$, (h) MuHH at $\theta = 150°$, and (i) MuHH at $\theta = 120°$.

uncertainties of the fitted surfaces. Such uncertainty underestimation, which can be quite dramatic, occurs whenever the system of equations solved during the optimization is ill determined; this is an especially serious concern when a large number of parameters are optimized. To confirm the quality of the fit, we also evaluated MUD, RMSD, and worst deviations for the test set of configurations not used during the fitting process, and these results are shown in Table 3. The MUDs and RMSDs observed on this test set are no worse than a factor of 2.1 times larger than those observed for the set of fitting data, and this confirms the high accuracy of the fitting process.

4. Analysis and Discussion

A set of contour plots for the final fitted diagonal corrections as functions of R_1 and R_2 for specific values of the included angle, θ, are displayed in Figure 3 for the DH_2, H_3, and MuH_2 isotopomers. The zero of energy of these plots is set to that of the minimum BODC at the D (or H or Mu) + H_2 asymptote, which occurs at $R_2 = 2.318$ a_0; this can be contrasted with the equilibrium separation of H_2 on either the BO or BH surfaces, both of which occur at $R_2 = 1.401$ a_0. When examining these plots, it is important to remember that they are not accurate when approaching the H + H + H limit where the ab initio BODC displays an extremely long-ranged interaction, whereas the fitted potentials have been damped to more rapidly approach the sum of the atomic BODC values. In Figure 4 the H_3 ab initio and fitted diagonal corrections along the collinear symmetric stretch are plotted to indicate the effect of the damping as the H + H + H limit is approached.

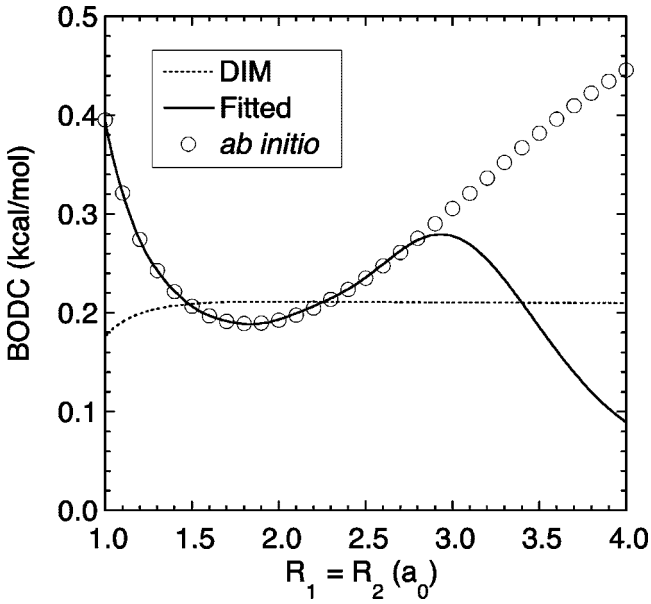

Figure 4. BODC (in kcal/mol) for H_3 along the collinear symmetric stretch relative to H + H_2 (R_{min}^{BODC}). The ab initio data are ill-behaved in the H + H + H limit, whereas the fitted functional representation is damped so that it goes to 3 times the atomic BODC.

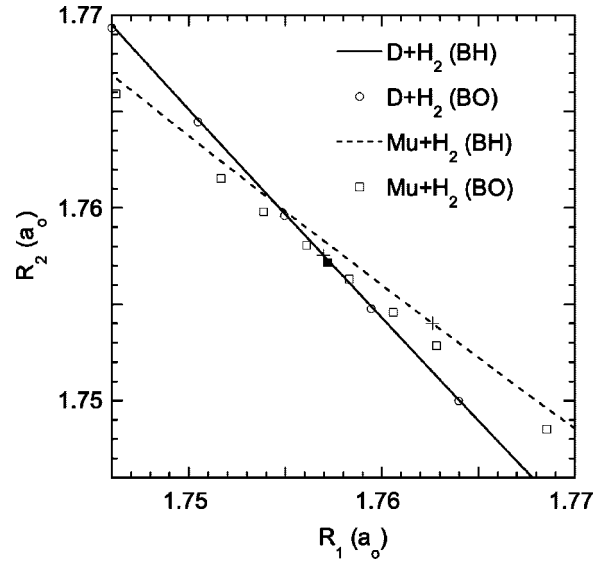

Figure 6. Values of the A−B distance (R_1) and B−C distance (R_2) along the reaction paths on the BH surfaces are denoted by lines for the D + H_2 (—) and Mu + H_2 (- - -) reactions. Reaction path geometries on the BO (CCI) surface are denoted by symbols for the D + H_2 (○) and Mu + H_2 (□) reactions. The solid square (■) denotes the saddle point for the BO surface, which is mass independent. The saddle points for the D + H_2 and Mu + H_2 reactions on the BH surfaces are denoted by plus signs (+). The saddle point for the Mu + H_2 reaction is furthest from the saddle point on the BO surface.

Perhaps the most striking feature observed in the H_3 and DH_2 contour plots of Figure 3 is that the BODC is large primarily in the strong interaction region; thus, it will have a significant effect on the barrier heights, which will influence the thermal rate constants, but will have less influence on other aspects of the dynamics. A convenient way to measure the effect of the BODC on inelastic scattering is to expand the BH potential, where the BO component is represented by the CCI PES, in a Legendre expansion

$$V(R, r, \gamma) = \sum_{n=0} V_{2n}(R, r) P_{2n}(\cos \gamma) \qquad (37)$$

where Jacobi coordinates are used; that is, r is the magnitude of the vector **r** that connects mass m_2 to mass m_3, R is the magnitude of the vector **R** connecting m_1 to the center of mass of diatom m_2-m_3, and γ is the angle between **r** and **R**. Low-energy inelastic scattering is sensitive to the shape of the first anisotropic expansion coefficient, $V_2(R, r)$. Figure 5 compares the behavior of $V_2(R, r)$ at $r = 1.4$ a_0 for the BO potential and for a selection of BH surfaces. The influence of the BODC on the potential anisotropy is observed to be quite modest.

In Table 4, we compare the saddle point properties of the fitted BH surfaces obtained by combining the new BODC representation with the BO CCI PES to the best available ab initio results; that is, the previously published[11] MRCI(11)/aug-cc-pV5Z//MRCI(3)/aug-cc-pVTZ BODC calculations combined with BO energies predicted via the CCI PES. The agreement is extremely good in all cases. We note that much of the remaining small differences observed in the barrier heights is due to

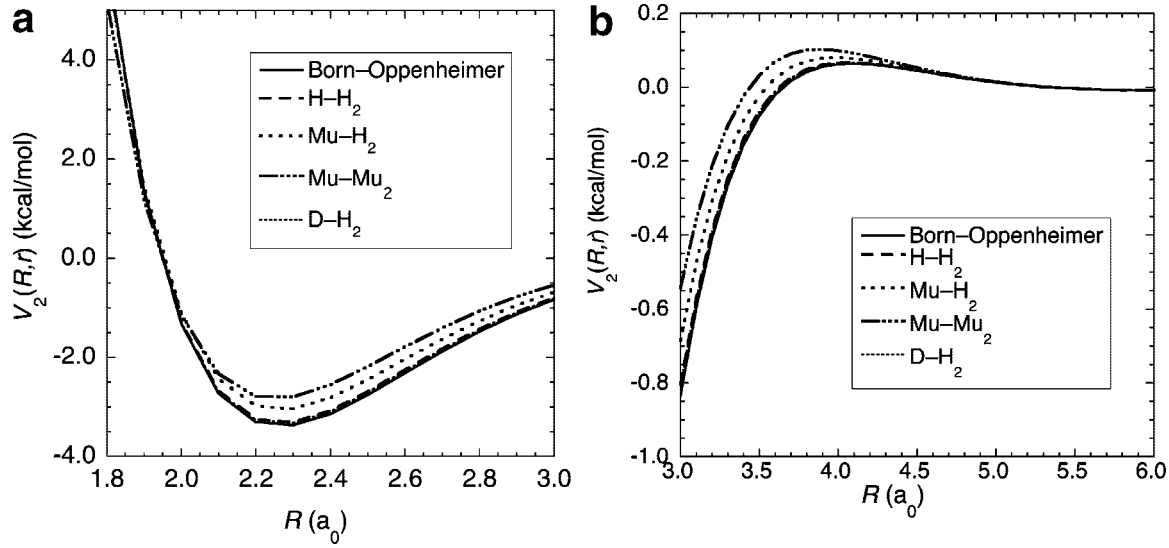

Figure 5. A comparison of the long-range behavior of the first anisotropic Legendre expansion coefficient for $r = 1.40$ a_0 for the BO PES and for various isotopomers on the BH PES: (a) 1.8 $a_0 < R < 3.0$ a_0 and (b) 3.0 $< R <$ 6.0 a_0.

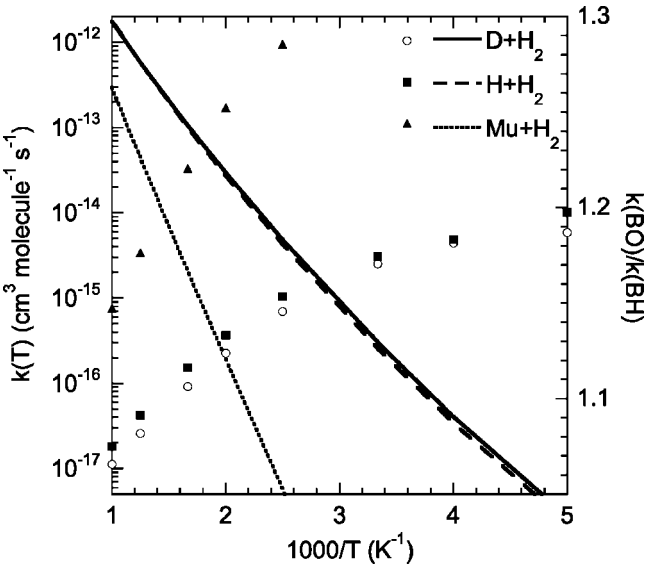

Figure 7. Temperature dependence of rate constants (left axis) computed on the BH surface are shown as lines for the D + H_2 (—), H + H_2 (— — —) and Mu + H_2 (- - -) reactions. Temperature dependence of ratios of rate constants computed on the BO surface and the BH surface (right axis) are shown as symbols for the D + H_2 (○), H + H_2 (■), and Mu + H_2 (▲) reactions.

TABLE 4: Comparison of the BH Saddle Point Geometries (a_0), Harmonic Frequencies (cm^{-1}), and Changes in the Barrier Height Due to the Diagonal Correction (cm^{-1}) for Various Isotopomers As Calculated with the Fitted Potential Surface and the Best Available Ab Initio Treatment, *i.e.*, the previously Published[11] MRCI(11)/aug-cc-pV5Z//MRCI(3)/aug-cc-pVTZ calculations[a]

system	method	R_1	R_2	ω_{sym}	ω_{bend}	ω_{asym}/i	$\Delta^{barrier}$
HHH	surface	1.7573	1.7573	2053	876	1533	53.70
	ab initio[a]	1.7573	1.7573	2053	876	1534	53.57
DDD	surface	1.7573	1.7573	1452	620	1074	26.86
	ab initio[a]	1.7572	1.7572	1452	620	1074	26.80
TTT	surface	1.7572	1.7572	1186	507	874	17.93
	ab initio[a]	1.7572	1.7572	1186	507	874	17.90
MuMuMu	surface	1.7583	1.7583	6128	2570	5245	477.20
	ab initio[a]	1.7581	1.7581	6134	2570	5264	476.14
DHH	surface	1.7570	1.7575	1767	839	1452	48.92
	ab initio[a]	1.7569	1.7575	1767	839	1452	48.80
THH	surface	1.7568	1.7576	1654	826	1416	47.31
	ab initio[a]	1.7568	1.7576	1654	826	1416	47.21
MuHH	surface	1.7626	1.7540	4280	1338	1894	129.29
	ab initio[a]	1.7626	1.7539	4280	1337	1898	128.39
HDD	surface	1.7576	1.7570	1765	670	1142	31.64
	ab initio[a]	1.7576	1.7570	1765	670	1143	31.57
MuDD	surface	1.7630	1.7537	4080	1212	1376	107.25
	ab initio[a]	1.7630	1.7536	4079	1211	1378	106.33

[a] Reference 11 [a] In both cases, the BO energies are determined with the CCI PES.

differences between the ab initio treatments used for the fitted data and the benchmark calculations rather than to fitting errors (for example, the MRCI(11)/aug-cc-pV5Z saddle point correction is about 0.15 cm^{-1} lower than the result predicted by the MRCI(3)/aug-cc-pVTZ results).

We employed variational transition state theory (VTST) with multidimensional tunneling corrections[53] to provide a first estimate of the importance of the diagonal correction on rate constants for the D + H_2, H + H_2, and Mu + H_2 reactions. The calculations were performed using the ABCRATE code.[53] A general description of VTST for calculations of reaction rates in triatomic systems with collinear reaction paths is given elsewhere.[54,55] Specifically, we used the improved canonical variation theory,[56] in which eigenvalues of the stretch mode (describing motion perpendicular to the reaction path) are computed by a WKB approximation,[57] and energy levels for the doubly degenerate bends are computed by the centrifugal oscillator approximation,[58,59] where the bend potential is fitted to a harmonic−quartic potential.[60] Quantum corrections for reaction coordinate motion are included by a multiplicative transmission coefficient that is computed from a normalized Boltzmann average of semiclassical tunneling probabilities.[61] The tunneling probabilities were computed using the least-action ground-state method.[62]

The collinear reaction paths for the BO and BH surfaces near the saddle points are displayed in Figure 6. The computed rate constants for the D + H_2, H + H_2, and Mu + H_2 reactions on the BH surface are displayed in Figure 7. For each reaction, we also show the ratio of the rate constant on the BO surface with that for the BH surface. The rate constants for D + H_2 and H + H_2 are similar, and the ratio of BO to BH rate constants varies from 1.2 to 1.06 over the temperature range 200 to 1000 K for these two reactions. For D + H_2, the VTST results are in good agreement with the results of accurate quantum scattering calculations[12] adjusted with a simple correction for the effect of the diagonal correction on the barrier; for temperatures above 200 K, the agreement is within 3−14%, whereas the VTST results are about 50% higher at 200 K. The rate constants for Mu + H_2 are much smaller than those for the other reactions, and the difference between the BO and BH results are larger. For example, the BO rate constant is predicted to be about 30% higher at 400 K. The Mu + H_2 system is a challenging system for VTST, and significant deviations between VTST[63] and quantum mechanical rate constants[64] have been observed; however, the ratios of the BO to BH rate constants are probably reasonably reliable. Accurate quantum mechanical calculations for the Mu + H_2 rate constants on the BO and BH PESs will be presented elsewhere.

5. Concluding Remarks

An accurate functional representation for the Born−Oppenheimer diagonal correction, fitted to data of essentially complete CI quality, has been presented that allows treatment of any desired isotopomer of H_3. This diagonal correction surface may be combined with any BO surface to yield Born−Huang PESs. Fortran routines are provided to facilitate evaluation of the energies and gradients of the BH surface obtained by adding the diagonal correction surface to the CCI PES. Variational transition state theory calculations were also presented to provide an initial assessment of the importance of accounting for the diagonal correction in the evaluation of thermal rate constants.

Acknowledgment. The authors are grateful to David Yarkony for helpful discussions. This work was supported by the National Science Foundation (Grant CHE-0111282 to K.A.P.), the Air Force Office of Scientific Research (Grant FA955D-07-1-0095 to G.C.S.), and the Chemical Sciences Division in the Office of Basic Energy Sciences of the U.S. Department of Energy. Part of this research was performed in the W. R. Wiley Environmental Molecular Sciences Laboratory, a national scientific user facility sponsored by the Department of Energy's Office of Biological and Environmental Research and located at Pacific Northwest National Laboratory. Pacific Northwest National Laboratory is operated for the Department of Energy by Battelle.

Supporting Information Available: Fortran routines of the fitted BODC surface interfaced with the CCI BO PES, including analytical gradients, are provided. This material is available free of charge via the Internet at http://pubs.acs.org.

References and Notes

(1) Schatz, G. C.; Kuppermann, A. *J. Chem. Phys.* **1976**, *65*, 4668.
(2) Kuppermann, A.; Schatz, G. C. *J. Chem. Phys.* **1975**, *62*, 2502.
(3) Truhlar, D. G.; Wyatt, R. E. *Annu. Rev. Phys. Chem.* **1976**, *27*, 1.
(4) Truhlar, D. G.; Wyatt, R. E. *Adv. Chem. Phys.* **1977**, *36*, 141.
(5) Banares, L.; Aoiz, F. J.; Herrero, V. J. *Phys. Scr.* **2006**, *73*, C6.
(6) Aoiz, F. J.; Banares, L.; Herrero, V. J. *Int. Rev. Phys. Chem.* **2005**, *24*, 119.
(7) Hu, W.; Schatz, G. C. *J. Chem. Phys.* **2006**, *125*, 132301.
(8) Born, M.; Oppenheimer, J. R. *Ann. Phys.* **1927**, *84*, 457.
(9) Mielke, S. L.; Garrett, B. C.; Peterson, K. A. *J. Chem. Phys.* **1999**, *111*, 3806.
(10) Mielke, S. L.; Garrett, B. C.; Peterson, K. A. *J. Chem. Phys.* **2002**, *116*, 4142.
(11) Mielke, S. L.; Schwenke, D. W.; Peterson, K. A. *J. Chem. Phys.* **2005**, *122*, 224313.
(12) Mielke, S. L.; Peterson, K. A.; Schwenke, D. W.; Garrett, B. C.; Truhlar, D. G.; Michael, J. V.; Su, M.-C.; Sutherland, J. W. *Phys. Rev. Lett.* **2003**, *91*, 063201.
(13) Ballhausen, C. J.; Hansen, A. E. *Annu. Rev. Phys. Chem.* **1972**, *23*, 15.
(14) Born, M.; Huang, K. *The Dynamical Theory of Crystal Lattices*; Clarendon Press: Oxford, 1954.
(15) Pack, R. T.; Hirschfelder, J. O. *J. Chem. Phys.* **1970**, *52*, 521.
(16) Golden, S. *Mol. Phys.* **1998**, *93*, 421.
(17) Czako, G.; Csaszar, A. G.; Szalay, V.; Sutcliffe, B. T. *J. Chem. Phys.* **2007**, 126.
(18) Truhlar, D. G.; Horowitz, C. J. *J. Chem. Phys.* **1978**, *68*, 2466.
(19) Varandas, A. J. C.; Brown, F. B.; Mead, C. A.; Truhlar, D. G.; Blais, N. C. *J. Chem. Phys.* **1987**, *86*, 6258.
(20) Boothroyd, A. I.; Keogh, W. J.; Martin, P. G.; Peterson, M. R. *J. Chem. Phys.* **1991**, *95*, 4343.
(21) Boothroyd, A. I.; Keogh, W. J.; Martin, P. G.; Peterson, M. R. *J. Chem. Phys.* **1996**, *104*, 7139.
(22) Dunning, T. H., Jr. *J. Chem. Phys.* **1989**, *90*, 1007.
(23) Kendall, R. A.; Dunning, T. H., Jr.; Harrison, R. J. *J. Chem. Phys.* **1992**, *96*, 6796.
(24) Riley, K. E.; Anderson, J. B. *J. Chem. Phys.* **2003**, *118*, 3437.
(25) Sellers, H.; Pulay, P. *Chem. Phys. Lett.* **1984**, *103*, 463.
(26) Handy, N. C.; Yamaguchi, Y.; Schaefer, H. F. *J. Chem. Phys.* **1986**, *84*, 4481.
(27) Ioannou, A. G.; Amos, R. D.; Handy, N. C. *Chem. Phys. Lett.* **1996**, *251*, 52.
(28) Garashchuk, S.; Light, J. C.; Rassolov, V. A. *Chem. Phys. Lett.* **2001**, *333*, 459.
(29) Schwenke, D. W. *J. Phys. Chem. A* **2001**, *105*, 2352.
(30) Valeev, E. F.; Sherrill, C. D. *J. Chem. Phys.* **2003**, *118*, 3921.
(31) Gauss, J.; Tajti, A.; Kallay, M.; Stanton, J. F.; Szalay, P. G. *J. Chem. Phys.* **2006**, *125*, 144111.
(32) Saxe, P.; Yarkony, D. R. *J. Chem. Phys.* **1987**, *86*, 321.
(33) Jensen, J. O.; Yarkony, D. R. *J. Chem. Phys.* **1988**, *89*, 975.
(34) Mitrushenkov, A. O.; Palmieri, P.; Puzzarini, C.; Tarroni, R. *Mol. Phys.* **2000**, *98*, 1677.
(35) Schwenke, D. W. *J. Chem. Phys.* **2003**, *118*, 6898.
(36) Tajti, A.; Szalay, P. G.; Gauss, J. *J. Chem. Phys.* **2007**, *127*, 014102.
(37) Wolniewicz, L. *J. Chem. Phys.* **1993**, *99*, 1851.
(38) Cencek, W.; Rychlewski, J.; Jaquet, R.; Kutzelnigg, W. *J. Chem. Phys.* **1998**, *108*, 2831.
(39) Cencek, W.; Kutzelnigg, W. *Chem. Phys. Lett.* **1997**, *266*, 383.
(40) Schwartz, C. *Phys. Rev.* **1962**, *126*, 1015.
(41) Carroll, D. P.; Silverstone, H. J.; Metzger, R. M. *J. Chem. Phys.* **1979**, *71*, 4142.
(42) Hill, R. N. *J. Chem. Phys.* **1985**, *83*, 1173.
(43) Kutzelnigg, W.; Morgan, J. D., III. *J. Chem. Phys.* **1992**, *96*, 4484.
(44) Knowles, P. J.; Werner, H.-J. *Chem. Phys. Lett.* **1988**, *145*, 514.
(45) Werner, H.-J.; Knowles, P. J. *J. Chem. Phys.* **1988**, *89*, 5803.
(46) Werner, H.-J.; Knowles, P. J. MOLPRO is a package of ab initio programs written by Werner H.-J and Knowles with contributions from Almlöf, J.; Amos, R. D.; Bernhardsson, A.; Berning, A.; Celani, P.; Cooper, D. L.; Deegan, M. J.; Dobbyn, A. J.; Eckert, F.; Elbert, S. T.; Hampel, C.; Hetzer, G.; Korona, T.; Lindh, R.; Lloyd, A. W.; McNicholas, S. J.; Manby, F. R.; Meyer, W.; Mura, M.; Nicklass, A.; Palmieri, P.; Peterson, K. A.; Pitzer, R. M.; Pulay, P.; Rauhut, G.; Schütz, M.; Stoll, H.; Stone, A. J.; Tarroni, R.; Taylor, P. R.; Thorsteinsson, T.
(47) Handy, N. C.; Lee, A. M. *Chem. Phys. Lett.* **1996**, *252*, 425.
(48) Murrell, J. N.; Carter, S.; Farantos, S. C.; Huxley, P.; Varandas, A. J. C. *Molecular Potential Energy Functions*; John Wiley and Sons: Chichester, 1984.
(49) Aguado, A.; Paniagua, M. *J. Chem. Phys.* **1992**, *96*, 1265.
(50) Garrett, B. C.; Truhlar, D. G. *J. Chem. Phys.* **1985**, *82*, 4543; **1986**, *84*, 7057E.
(51) Mead, C. A. *J. Chem. Phys.* **1983**, *78*, 807.
(52) Thompson, D. L.; Blais, N. C.; Truhlar, D. G. *J. Chem. Phys.* **1983**, *78*, 1335.
(53) Garrett, B. C.; Lynch, G. C.; Allison, T. C.; Truhlar, D. G. *Comput. Phys. Commun.* **1998**, *109*, 47.
(54) Garrett, B. C.; Truhlar, D. G. *J. Am. Chem. Soc.* **1979**, *101*, 4534.
(55) Garrett, B. C.; Truhlar, D. G. *J. Chem. Phys.* **1980**, *72*, 3460.
(56) Garrett, B. C.; Truhlar, D. G.; Grev, R. S.; Magnuson, A. W. *J. Phys. Chem.* **1980**, *84*, 1730.
(57) Garrett, B. C.; Truhlar, D. G. *J. Chem. Phys.* **1984**, *81*, 309.
(58) Natanson, G. A. *J. Chem. Phys.* **1990**, *93*, 6589.
(59) Garrett, B. C.; Truhlar, D. G. *J. Phys. Chem.* **1991**, *95*, 10374.
(60) Garrett, B. C.; Truhlar, D. G. *J. Phys. Chem.* **1979**, *83*, 1915.
(61) Garrett, B. C.; Truhlar, D. G. *J. Phys. Chem.* **1979**, *83*, 2921.
(62) Garrett, B. C.; Truhlar, D. G. *J. Chem. Phys.* **1983**, *79*, 4931.
(63) Garrett, B. C.; Steckler, R.; Truhlar, D. G. *Hyperfine Interact.* **1986**, *32*, 779.
(64) Schatz, G. C. *J. Chem. Phys.* **1985**, *83*, 3441.

JP8110887